

Coupling Bright and Dark Plasmonic Lattice Resonances

S. R. K. Rodriguez,^{1,*} A. Abass,² B. Maes,³ O. T.

A. Janssen,⁴ G. Vecchi,¹ and J. Gómez Rivas^{1,5}

¹*Center for Nanophotonics, FOM Institute AMOLF,
c/o Philips Research Laboratories, High Tech Campus 4,
5656 AE Eindhoven, The Netherlands*

²*Department of Electronic and Information Systems (ELIS),
Ghent University, Sint-Pietersnieuwstraat 41, B-9000 Ghent, Belgium*

³*Micro- and Nanophotonic Materials Group,
Institut de Physique, University of Mons,
Place du Parc 20, B-7000 Mons, Belgium*

⁴*Optics Research Group, Delft University of Technology, 2628 CJ Delft, The Netherlands*

⁵*Department of Applied Physics, Eindhoven University of Technology,
P.O. Box 513, 5600 MB Eindhoven, The Netherlands*

(Dated: August 9, 2011)

Abstract

We demonstrate the coupling of bright and dark Surface Lattice Resonances (SLRs), which are collective Fano resonances in 2D plasmonic crystals. As a result of this coupling, a frequency stop-gap in the dispersion relation of SLRs is observed. The different field symmetries of the low and high frequency SLR bands lead to pronounced differences in their coupling to free space radiation. Standing waves of very narrow spectral width compared to localized surface plasmon resonances are formed at the high frequency band edge, while subradiant damping onsets at the low frequency band edge leading the resonance into darkness. We introduce a coupled oscillator analog to the plasmonic crystal, which serves to elucidate the physics of the coupled plasmonic resonances and to estimate very high quality factors ($Q > 700$) for SLRs, which are the highest known for any 2D plasmonic crystal.

PACS numbers: 73.20.Mf, 42.25.Fx, 71.36.+c, 78.67.Bf

* s.rodriguez@amolf.nl

Metallic nanoparticles supporting surface plasmon resonances allow light to be localized in nanoscale volumes, thereby opening exciting possibilities such as nanoscale control of emitters [1], large electromagnetic enhancements [2], and nonlinear nano-optics [3]. Much attention has been given to Localized Surface Plasmon Resonances (LSPRs), which arise in individual particles when their conduction electrons are coherently driven by an electromagnetic field. Although localized surface plasmons may couple, their resonances are in general severely broadened due to strong radiative damping and hence exhibit low quality factors Q . A recent development in nanoplasmonics deals with collective resonances in periodic arrays of metallic nanostructures, or plasmonic crystals. Such arrays support Surface Lattice Resonances (SLRs), which are collective resonances mediated by diffractive coupling of localized plasmons. This coupling occurs near the critical frequency when a radiating diffraction order becomes evanescent, i.e., at the Rayleigh anomaly. SLRs were introduced by Carron [4], and the interest in this phenomenon was revived by Schatz and co-workers with a series of works on 1D and 2D arrays [5, 6]. However, the experimental observation of SLRs was elusive for many years [7]. Recent advances in nano-fabrication and in the understanding of SLRs have allowed for their observation in periodic arrays of nanostructures with different geometries [8–13]. In contrast with LSPRs, SLRs possess much higher Q s, and the associated polaritons can propagate over tens of unit cells in the plasmonic crystal [12]. The relevance of SLRs for enhanced, directional, and polarized light emission [11, 14] and sensing [15] has been recently demonstrated. Although the coupling of surface modes in periodic metallic structures has attracted much interest [16–19], especially for its connection with frequency stop-gaps [20], coupled SLRs have not been discussed yet.

In this paper, we demonstrate the mutual coupling of SLRs and the formation of a frequency stop-gap in the dispersion relation of these modes. This coupling leads to a strong modification of the SLRs characteristics, including the onset of subradiant damping in the low frequency band, zero group velocity modes in the high frequency band, and Q -factors for both bands which are amongst the highest reported for any 2D plasmonic crystal. Our results set the basis for controlling the dispersion of SLRs, and they open new possibilities in sensing, enhanced spontaneous light emission, and lasing at the band edges of SLR gaps.

We have investigated $3 \times 3 \text{ mm}^2$ arrays of gold nanorods fabricated on a silica substrate using substrate conformal imprint lithography (SCIL) [21]. A top view SEM image of an array is displayed in the inset of Figure 1. This array has rods with dimensions $450 \times 120 \times 38$

nm³ arranged in a lattice with constants $a_x = 600$ nm and $a_y = 300$ nm. The array was embedded in a uniform surrounding medium by placing a silica superstrate preceded with $n=1.45$ index matching fluid to ensure good optical contact. We measured the variable angle transmittance of the collimated beam from a halogen lamp while rotating the sample around the y-axis. The polarization of the incident light was set along the y-axis, probing the short axis of the nanorods. For this polarization the dipolar LSPR lies at higher energies than the $(\pm 1, 0)$ diffraction orders, thereby allowing the coupling of localized surface plasmons to these orders [8].

Figure 1 displays the extinction of the array defined as $1 - T$, with T the transmittance, as a function of the reduced frequency, i.e., the angular frequency normalized by the speed of light in vacuum, and the projection of the incident wave vector onto the surface of the array $k_{\parallel} = \frac{\omega}{c} \sin(\theta) \hat{x}$, with θ the angle of incidence. The broad, dispersionless extinction peak centered at a frequency near 9 mrad/nm corresponds to the excitation of LSPRs in the individual nanorods. The sharp, dispersive peaks at lower frequencies correspond to the excitation of SLRs. The $(\pm 1, 0)$ Rayleigh anomalies, which are the conditions for which the $(\pm 1, 0)$ diffracted orders are grazing to the surface, are indicated with solid lines in Figure 1. The coupling of localized surface plasmons to the Rayleigh anomalies is the origin of the observed SLRs.

A salient feature in the measurements of Figure 1 is the formation of a stop-gap centered at $\omega/c = 6.85$ mrad/nm and near $k_{\parallel} = 0$, where the two SLRs mutually couple. We note that this is not a complete photonic bandgap, since it exists for y-polarized light only. The gap arises from the coupling of two counter-propagating surface polaritons which, due to the structural anisotropy of both the nanorods and the lattice, have a strong polarization dependence on their coupling to free space radiation. At the high frequency band edge, we observe that the dispersion of the $(+1, 0)$ SLR flattens. This flattening of the band can be translated as a reduction of the mode's group velocity and the formation of standing waves, which are also associated with an increased density of optical states. At the low frequency band edge, the $(-1, 0)$ SLR becomes weaker and narrower. This behavior is characteristic of a mode tending towards subradiance, where radiative damping is suppressed in a collective state with an antisymmetric wave function [22]. As shown in nanoslit arrays [18], there is an intimate connection between subradiant damping and the opening of a gap in the dispersion relation of surface plasmon polaritons (SPPs).

Figure 2(a) shows a close view of the stop-gap in Figure 1, and Figure 2(b) shows results from finite element simulations (COMSOL). For the simulations we used a constant refractive index of 1.45 for silica, the permittivity of gold as given in Ref. [23], and Bloch-Floquet boundary conditions. The transmittance was calculated as the ratio between the transmitted power through the array and the incident power. In Figures 2(c) and (d) we compare simulations with measurements at $k_{\parallel} = 0$ and $k_{\parallel} = 0.4$ mrad/nm, respectively. By reproducing the measured dispersion of SLRs and the gap's central frequency and width, a good qualitative agreement between measurements and simulations is demonstrated. Discrepancies in the amplitude and spectral width of the resonances can be mainly attributed to differences between the simulated and fabricated geometries, especially near the corners.

It can be appreciated in Figures 1 and 2 that the SLR peaks together with the Rayleigh anomaly dips give rise to asymmetric resonance lineshapes, which can be understood in the framework set forth by Fano [24]. Fano described the quantum interference between a discrete state and a continuum of states as the origin of asymmetric resonance lineshapes. It was later shown in metallic subwavelength hole arrays that the coupling of surface plasmons to Rayleigh anomalies leads to similar lineshapes, with the resonantly scattered light acting as the discrete state and the background transmission as the continuum [25]. A similar situation is observed in our configuration. The broad dipolar LSPR determines the extent of background transmission, i.e. the continuum, according to its frequency difference with the Rayleigh anomaly. The Rayleigh anomaly corresponds to the discrete state. The diffractive coupling of localized surface plasmons therefore resembles the interaction between a continuum of states and a discrete state, leading to asymmetric resonance line shapes. As seen in Figures 1 and 2, the degree of asymmetry of these line shapes changes depending on the frequency and k-vector of excitation. This dependency is rooted in the relative contributions of resonant and non resonant scattering [26], which also manifest as a modification of the SLR damping; the latter point will be addressed further in the text.

The different electrodynamic response leading to the bright and dark character - efficient and inefficient coupling to light - of the (+1,0) and (-1,0) SLRs, respectively, transpires from the near-field enhancement and surface charge distribution of the nanorods at the respective frequencies. In Figure 3 we show simulation results for $k_{\parallel} = 0.4$ mrad/nm at two frequencies: $\omega/c = 7.1$ mrad/nm and $\omega/c = 6.7$ mrad/nm, which correspond to the (+1,0) and (-1,0) SLR, respectively. The small angle of incidence was chosen such that the extinction is not

negligible for the $(-1,0)$ SLR. Both plots are at a plane parallel to the array located at the mid-height of the nanorods. Charges of opposite sign at the surface of the nanorods are plotted in white and black, while the total near-field enhancement, i.e., $|E|^2/|E_0|^2$ with E the total field and E_0 the incident field, is displayed by the color scale. Figure 3 illustrates how the different resonant response has its origin in the symmetry of the modes. In order to couple to the incident plane wave at normal incidence, the mode has to be symmetric with respect to the plane defined by the incident k - and polarization vectors intersecting the nanorods along their center, i.e. the symmetry plane indicated by the dotted lines in Figure 3. The $(+1,0)$ mode, which is shown in Figure 3(a) for a small angle of incidence, has symmetric field and charge distributions with respect to the symmetry plane. A strong dipole moment is seen for each nanorod, and a strong dipolar inter-rod coupling takes places along the y -direction also. This results in a large extinction and an efficient coupling of the $(+1,0)$ mode to normal incidence light, as it can be appreciated in Figure 1. In contrast, the $(-1,0)$ mode has an antisymmetric field and charge distribution for $k_{\parallel} = 0$; the net dipole moment is therefore zero and the extinction vanishes. This symmetry is broken for angles of incidence larger than $\theta = 0^\circ$, thus allowing the excitation of this resonant mode as shown in Figure 3(b). The broken symmetry manifests as a quadrupolar surface charge distribution displaced from the symmetry axis. This results in a nonzero intra-rod and inter-rod dipole moment, which can be recognized from the charges of opposite sign inside the nanorods and for adjacent nanorods along the symmetry axis, respectively.

The coupled nature of SLRs can be elucidated by making an analogy with a set of three mutually coupled harmonic oscillators. Coupled oscillators have proven useful in understanding electromagnetic phenomena [27, 28]. In this analogy, the conduction electrons in the nanorods driven by the electromagnetic field are modeled as oscillator 1 driven by a harmonic force $F = F_0 e^{-i\omega_s t}$, whereas the $(+1,0)$ and $(-1,0)$ Rayleigh anomalies are modeled by oscillators 2 and 3, respectively. The equations of motion for the system are

$$\begin{aligned} \ddot{x}_1 + \gamma_1 \dot{x}_1 + \omega_1^2 x_1 - \Omega_{12}^2 x_2 - \Omega_{13}^2 x_3 &= F, \\ \ddot{x}_2 + \gamma_2 \dot{x}_2 + \omega_2^2 x_2 - \Omega_{12}^2 x_1 - \Omega_{23}^2 x_3 &= 0, \\ \ddot{x}_3 + \gamma_3 \dot{x}_3 + \omega_3^2 x_3 - \Omega_{13}^2 x_1 - \Omega_{23}^2 x_2 &= 0, \end{aligned} \tag{1}$$

where x_j , γ_j , and ω_j ($j = 1, 2, 3$) are the displacement from equilibrium position, damping, and eigenfrequency associated with the j^{th} oscillator, respectively, and Ω_{jk}

TABLE I. The Ω_{jk} terms ($j, k = 1, 2, 3$ and $j \neq k$) are the coupling frequencies between the j^{th} and k^{th} oscillators, and the γ_j terms are the damping frequencies associated with the j^{th} oscillator, for the system described by Equation 1. All quantities are given in units of mrad/nm. In the entries for which a minimum estimate is given, the value in parenthesis represents the value yielding the spectra in Figure 4.

	Ω_{12}	Ω_{13}	Ω_{23}	γ_2	γ_3
$k_{\parallel}=0$	2.8 ± 0.1	-	-	<0.01 (0.001)	-
$k_{\parallel}=0.17$	3.1 ± 0.1	<0.6 (0.1)	1.1 ± 0.1	0.02 ± 0.01	0.020 ± 0.005
$k_{\parallel}=0.68$	3.3 ± 0.1	2.4 ± 0.1	<0.7 (0.3)	0.06 ± 0.02	0.03 ± 0.01

($k = 1, 2, 3$ and $j \neq k$) is the coupling frequency between the j^{th} and k^{th} oscillator. Since we are interested in the extinct optical power in driving the electrons in the nanorod, we calculate the absorbed mechanical power by oscillator 1 from the driving force, which is given by $P(t) = F\dot{x}_1$. Integrating $P(t)$ over one period of oscillation and scanning the driving frequency ω_s yields an absorbed power spectrum $P(\omega_s)$, which is representative of the extinction spectrum.

In Figure 4 we compare $P(\omega_s)$ with the measured extinction spectra at three values of k_{\parallel} . In all three cases $\omega_1 = 9.25$ mrad/nm and $\gamma_1 = 2.3$ mrad/nm, which reproduce the frequency and damping of the LSPR, and $F_0 = 0.57$ units of force per mass is a fitting parameter determining the amplitude of the spectra. The eigenfrequencies ω_2 and ω_3 are determined for each value of k_{\parallel} by the corresponding $(\pm 1, 0)$ Rayleigh anomalies of the array. The remaining parameters, i.e., coupling and damping frequencies associated with the lattice modes, are the parameters used to fit the measured SLR lineshapes and are given in Table 1 for three values of k_{\parallel} .

Figure 4(a) displays the spectra at $k_{\parallel} = 0$, where the Rayleigh anomalies are degenerate at $\omega_2 = 7.26$ mrad/nm and the $(-1, 0)$ SLR is a dark state. In this case the model reduces to that of two coupled oscillators. With increasing k_{\parallel} the $(-1, 0)$ SLR comes out of the darkness, so the three oscillators are mutually coupled. In Figure 4(b) we consider the case $k_{\parallel} = 0.17$ mrad/nm, where $\omega_2 = 7.33$ mrad/nm and $\omega_3 = 6.92$ mrad/nm. From the values given in Table 1 we see that with respect to the normal incidence case, at $k_{\parallel} = 0.17$ mrad/nm the nanorods are more strongly coupled to the $(+1, 0)$ Rayleigh anomaly (Ω_{12}

increases), only weakly coupled to the (-1,0) Rayleigh anomaly (low Ω_{13}), the Rayleigh anomalies are mutually coupled (high Ω_{23}), and the damping of both resonances has very significantly increased (both γ_2 and γ_3 increase). Further increasing to $k_{\parallel} = 0.68$ mrad/nm makes $\omega_2 = 7.68$ mrad/nm and $\omega_3 = 6.70$ mrad/nm, which is the case in Figure 4(c). At this value of k_{\parallel} there is an increased coupling of the nanorods to both Rayleigh anomalies (both Ω_{12} and Ω_{13} increase), the coupling between the Rayleigh anomalies decreases (Ω_{23} decreases), and the damping of both resonances increases (both γ_2 and γ_3 increase).

From the above mentioned behaviors and the quantities given in Table 1 we are able to draw several conclusions. Firstly, the model shows how the coupling terms Ω_{jk} determine the frequency difference between the SLR peaks and the Rayleigh anomalies as evidenced in Figure 1. Namely, for the (+1,0) Rayleigh anomaly we observe that as k_{\parallel} increases the SLR peak deviates more in frequency. This behavior is defined in the increase of Ω_{12} which detunes the resonance peak from the Rayleigh anomaly. In contrast, for the (-1,0) diffraction order we observe a decreasing frequency deviation of the SLR from its corresponding Rayleigh anomaly as k_{\parallel} increases. In this case the dominant interaction near normal incidence is the mutual coupling of SLRs described by the term Ω_{23} , which detunes the (-1,0) SLR from its Rayleigh anomaly at low k_{\parallel} . Although $\Omega_{13} > \Omega_{23}$ at large values of k_{\parallel} , at low values of k_{\parallel} the Ω_{23} interaction dominates due to the smaller frequency difference between the eigenfrequencies ω_3 and ω_2 . Secondly, the model shows that the damping of both resonances increases with k_{\parallel} , which leads to less asymmetric Fano lineshapes and broader linewidths for both resonances. The decreasingly asymmetric lineshapes as k_{\parallel} increases are especially clear in Figure 4, whereas the SLR broadening and variable extinction of the Rayleigh anomalies are visible in Figure 1.

It is interesting to calculate the Q -factors of the uncoupled oscillators, which follow from the definition $Q_j = \omega_j/\gamma_j$. For oscillator 1 resonating at the LSPR frequency we obtain $Q_1 = 4$. For oscillator 2 yielding the (+1,0) SLR, we have $Q_2 > 700$ at normal incidence. This value, which is to the best of our knowledge higher than any reported Q for an experimental study on 2D plasmonic crystals, is a minimum limit. This limit arises because for any value $\gamma_2 < 0.01$ a fit to the measurement within a 10% uncertainty in the magnitude of the extinction can be obtained. For oscillator 3 yielding the (-1,0) SLR, we have $Q_3 = 300$ at $k_{\parallel} = 0.17$ mrad/nm. It is important to realize that the resonances in the coupled system exhibit an effective damping which is not equal to the damping of the

uncoupled oscillators. Nevertheless, the above values clearly reflect the large differences in Q -factors between LSPRs and SLRs. Furthermore, the coupled oscillator model points to the origin of the narrow SLR linewidths, which is the coupling of two harmonic oscillators with very different damping. By comparing Q_1 and Q_3 with previously reported experimental data, we get an insight into how well the Q -factors of the uncoupled oscillators represent the Q -factors of the resonances in the coupled system. Firstly, $Q_1 = 4$ is a typical result for LSPRs with high radiative damping [29]. Secondly, in Ref. [18] Ropers and co-workers measured for subradiantly damped SPPs in a nanoslit array near a stop-gap (similar to what we observe for the $(-1,0)$ SLR near the gap) lifetimes near $\tau = 200$ fs. Nanoslits can be represented quite accurately as resonators [30], so the lifetime of the excited state, τ , is related to Q by $Q = 2\pi\nu\tau$, with ν the frequency. Inserting $\tau = 200$ fs and $\nu = 400$ THz (the frequency of the subradiant mode in Ref. [18]) yields $Q = 500$, which is comparable with the value that we find, i.e., $Q_3 = 300$. Despite the differences in the structures considered and possibly the extent of subradiant damping, it is remarkable that the oscillator model yields at the very least an order of magnitude estimate for the Q of a nearly subradiant SPP mode in the vicinity of a stop-gap. It should be mentioned that for arrays of dimensions on the order of 10 microns or less, the Q -factors of SLRs are expected to appreciably decrease. This length scale corresponds to the associated surface polariton propagation lengths, which were recently determined in Ref. [12]. For arrays much larger than this characteristic length, such as the one herein considered, the Q -factor saturates. The inhibition of radiative damping that leads to a narrowing of the SLR linewidth is therefore a collective effect, i.e. it depends on the number of particles present in the array.

In conclusion, we have demonstrated the coupling of SLRs and the associated opening of a frequency stop-gap in the dispersion relation of these modes. The symmetric and antisymmetric field/charge distributions responsible for the bright and dark nature of the $(+1,0)$ and $(-1,0)$ modes, respectively, were illustrated. We have also estimated the very high quality factors of SLRs ($Q > 700$), which are to the best of our knowledge the highest reported values for any experimental study on 2D plasmonic crystals. Coupled bright and dark collective modes, as well as stop-gaps, offer the possibility to carefully design abrupt changes in the Local Density of Optical States (LDOS) over narrow spectral regions and in an extended volume. LDOS manipulation in plasmonic structures is relevant for enhancing the efficiency of light emitting devices (LEDs), sensors, and nonlinear processes, all of

which can be tailored in a frequency, angle, and polarization dependent manner with coupled SLRs. Moreover, the standing waves formed at the high frequency band edge hold exciting properties for the manipulation of light at the nanoscale since they have zero group velocity while being much less damped than LSPRs. Finally, we envisage that the strong suppression of radiative losses herein discussed holds great promise for the development of high Q distributed feedback surface polariton lasers and plasmonic sensors with enhanced sensitivity.

We thank V. Giannini and M. C. Schaafsma for fruitful discussions, M. Verschuuren and Y. Zhang for assistance in the fabrication of the samples. This work was supported by the Netherlands Foundation Fundamenteel Onderzoek der Materie (FOM) and the Nederlandse Organisatie voor Wetenschappelijk Onderzoek (NWO), and is part of an industrial partnership program between Philips and FOM.

-
- [1] O. L. Muskens, V. Giannini, J. A. Sánchez-Gil, and J. Gómez Rivas, “Strong Enhancement of the Radiative Decay Rate of Emitters by Single Plasmonic Nanoantennas,” *Nano Lett.* **7**, 2871–2875 (2007).
 - [2] J. Aizpurua, Garnett W. Bryant, Lee J. Richter, F. J. García de Abajo, Brian K. Kelley, and T. Mallouk, “Optical properties of coupled metallic nanorods for field-enhanced spectroscopy,” *Phys. Rev. B* **71**, 235420 (2005).
 - [3] Stefano Palomba, Matthias Danckwerts, and Lukas Novotny, “Nonlinear plasmonics with gold nanoparticle antennas,” *J. Opt. A* **11**, 114030 (2009).
 - [4] K. T. Carron, W. Fluhr, M. Meier, A. Wokaun, and H. W. Lehmann, “Resonances of two-dimensional particle gratings in surface-enhanced Raman scattering,” *J. Opt. Soc. Am. B* **3**, 430–440 (1986).
 - [5] Shengli Zou, Nicolas Janel, and George C. Schatz, “Silver nanoparticle array structures that produce remarkably narrow plasmon lineshapes,” *J. Chem. Phys.* **120**, 10871–10875 (2004).
 - [6] Shengli Zou and George C. Schatz, “Silver nanoparticle array structures that produce giant enhancements in electromagnetic fields,” *Chem. Phys. Lett.* **403**, 62 – 67 (2005).
 - [7] Erin M. Hicks, Shengli Zou, George C. Schatz, Kenneth G. Spears, Richard P. Van Duyne, Linda Gunnarsson, Tomas Rindzevicius, Bengt Kasemo, and Mikael Käll, “Controlling Plas-

- mon Line Shapes through Diffractive Coupling in Linear Arrays of Cylyndircal Nanoparticles Fabricated by Electron Beam Lithography,” *Nano Lett.* **5**, 1065–1070 (2005).
- [8] Baptiste Auguié and William L. Barnes, “Collective Resonances in Gold Nanoparticle Arrays,” *Phys. Rev. Lett.* **101**, 143902 (2008).
 - [9] Yizhuo Chu, Ethan Schonbrun, Tian Yang, and Kenneth B. Crozier, “Experimental observation of narrow surface plasmon resonances in gold nanoparticle arrays,” *Appl. Phys. Lett.* **93**, 181108 (2008).
 - [10] V. G. Kravets, F. Schedin, and A. N. Grigorenko, “Extremely Narrow Plasmon Resonances Based on Diffraction Coupling of Localized Plasmons in Arrays of Metallic Nanoparticles,” *Phys. Rev. Lett.* **101**, 087403 (2008).
 - [11] G. Vecchi, V. Giannini, and J. Gómez Rivas, “Shaping the Fluorescent Emission by Lattice Resonances in Plasmonic Crystals of Nanoantennas,” *Phys. Rev. Lett.* **102**, 146807 (2009).
 - [12] G. Vecchi, V. Giannini, and J. Gómez Rivas, “Surface modes in plasmonic crystals induced by diffractive coupling of nanoantennas,” *Phys. Rev. B* **80**, 201401 (2009).
 - [13] Andreas Bitzer, Jan Wallauer, Hannes Merbold, Hanspeter Helm, Thomas Feurer, and Markus Walther, “Lattice modes mediate radiative coupling in metamaterial arrays,” *Opt. Exp.* **17**, 22108–22113 (2009).
 - [14] V. Giannini, G. Vecchi, and J. Gómez Rivas, “Lighting Up Multipolar Surface Plasmon Polaritons by Collective Resonances in Arrays of Nanoantennas,” *Phys. Rev. Lett.* **105**, 266801 (2010).
 - [15] Peter Offermans, Martijn C. Schaafsma, Said R. K. Rodriguez, Yichen Zhang, Mercedes Crego-Calama, Sywert H. Brongersma, and Jaime Gómez Rivas, “Universal Scaling of the Figure of Merit of Plasmonic Sensors,” *ACS Nano* **5**, 5151–5157 (2011).
 - [16] S. C. Kitson, William L. Barnes, and J. R. Sambles, “Full Photonic Band Gap for Surface Modes in the Visible,” *Phys. Rev. Lett.* **77**, 2670–2673 (1996).
 - [17] C. Sauvan, C. Billaudeau, S. Collin, N. Bardou, F. Pardo, J.-L. Pelouard, and Lalanne P., “Surface plasmon coupling on metallic film perforated by two-dimensional rectangular hole array,” *Appl. Phys. Lett.* **92**, 011125 (2008).
 - [18] C. Ropers, D. J. Park, G. Stibenz, G. Steinmeyer, J. Kim, D. S. Kim, and C. Lienau, “Femtosecond Light Transmission and Subradiant Damping in Plasmonic Crystals,” *Phys. Rev. Lett.* **94**, 113901 (2005).

- [19] Amitabh Ghoshal, Ivan Divliansky, and Pieter G. Kik, “Experimental observation of mode-selective anticrossing in surface-plasmon-coupled metal nanoparticle arrays,” *Appl. Phys. Lett.* **94**, 171108 (2009).
- [20] W. L. Barnes, T. W. Preist, S. C. Kitson, and J. R. Sambles, “Physical origin of photonic energy gaps in the propagation of surface plasmons on gratings,” *Phys. Rev. B* **54**, 6227–6244 (1996).
- [21] Marc A. Verschuuren, Substrate Conformal Imprint Lithography for Nanophotonics, Ph.D. thesis, Utrecht University (2010).
- [22] R. H. Dicke, “Coherence in Spontaneous Radiation Processes,” *Phys. Rev.* **93**, 99–110 (1954).
- [23] Edward D. Palik, Handbook of optical constants of solids (Academic Press, New York, 1985).
- [24] U. Fano, “Effects of Configuration Interaction on Intensities and Phase Shifts,” *Phys. Rev.* **124**, 1866 (1961).
- [25] C. Genet, M. P. van Exter, and J. P. Woerdman, “Fano-type interpretation of red shifts and red tails in hole array transmission spectra,” *Opt. Comm.* **225**, 331–336 (2003).
- [26] M. Galli, S. L. Portalupi, M. Belotti, L. C. Andreani, L. O’Faolain, and T. F. Krauss, “Light scattering and Fano resonances in high-Q photonic crystal nanocavities,” *Appl. Phys. Lett.* **94**, 071101 (2009).
- [27] C. L. Garrido Alzar, M. A. G. Martinez, and P. Nussenzveig, “Classical analog of electromagnetically induced transparency,” *Am. J. Phys.* **70**, 37–41 (2002).
- [28] Shaunak Mukherjee, Heidar Sobhani, J. Britt Lassiter, Rizia Bardhan, Peter Nordlander, and Naomi J. Halas, “Fanoshells: Nanoparticles with Built-in Fano Resonances,” *Nano Lett.* **10**, 2694–2701 (2010).
- [29] S. A. Maier, Plasmonics: Fundamentals and Applications (Springer, New York, USA, 2007).
- [30] Sergey I. Bozhevolnyi and Thomas Søndergaard, “General properties of slow-plasmon resonant nanostructures: nano-antennas and resonators,” *Opt. Exp.* **15**, 10869–10877 (2007).

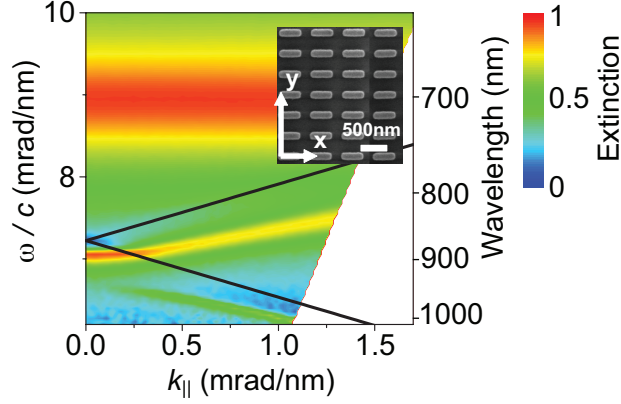


FIG. 1. (Color) Extinction spectra as a function of k_{\parallel} for y-polarized light incident on the array of gold nanorods shown in the inset. The black lines with positive and negative slope indicate the $(+1, 0)$ and $(-1, 0)$ Rayleigh anomalies, respectively. The dispersionless resonance at 9 mrad/nm is the dipolar localized surface plasmon resonance for the short-axis of the nanorods, whereas the narrower and dispersive resonances below the Rayleigh anomalies are the surface lattice resonances.

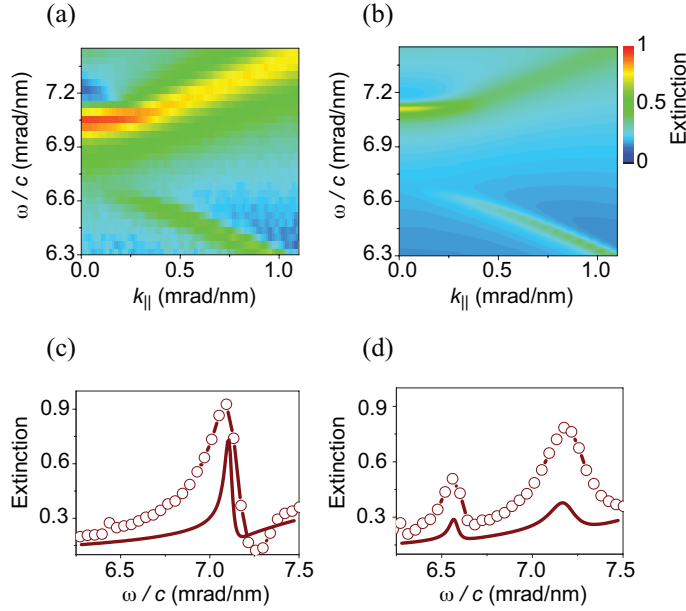


FIG. 2. (Color) Measurements (a) and finite element simulations (b) of the extinction spectra of the array shown in Figure 1. Figures (c) and (d) are cuts at $k_{\parallel} = 0$ and $k_{\parallel} = 0.4$ mrad/nm, respectively, of both (a) and (b). The open circles in (c) and (d) are measurements and the solid curves are simulations.

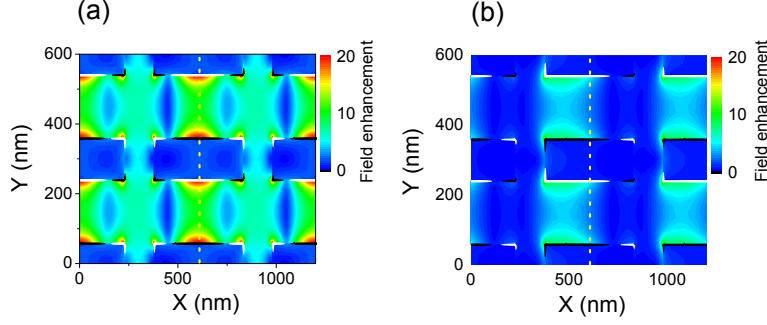


FIG. 3. (Color) Near field enhancement in color scale and surface charge distribution (at an arbitrary phase) in black and white at the mid-height of the nanorods for the $(+1,0)$ (a) and $(-1,0)$ (b) surface lattice resonance at $k_{\parallel} = 0.4$ mrad/nm. The dotted lines indicate the plane of symmetry for coupling to radiation.

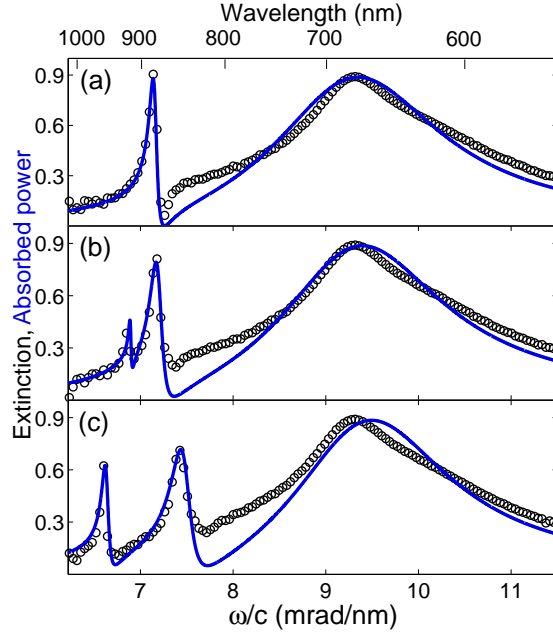


FIG. 4. The black open circles are cuts of the measured extinction spectra shown in Figure 1 at three values of k_{\parallel} : (a) $k_{\parallel} = 0$ mrad/nm, (b) $k_{\parallel} = 0.17$ mrad/nm, and (c) $k_{\parallel} = 0.68$ mrad/nm. The blue solid curves represent the absorbed power in oscillator 1 of the coupled oscillator model described in the text, with coupling and damping frequencies as given in Table 1.